LETTERS
PUBLISHED ONLINE: 8 JUNE 2015 | DOI: 10.1038/NMAT4298
nature materials

Liquid-crystalline ordering of antimicrobial peptide–DNA complexes controls TLR9 activation

Nathan W. Schmidt[1†], Fan Jin[1,2†], Roberto Lande[3,4†], Tine Curk[5†], Wujing Xian[1], Calvin Lee[1], Loredana Frasca[3,4], Daan Frenkel[5], Jure Dobnikar[5,6,7*], Michel Gilliet[3*] and Gerard C. L. Wong[1*]

Double-stranded DNA (dsDNA) can trigger the production of type I interferon (IFN) in plasmacytoid dendritic cells (pDCs) by binding to endosomal Toll-like receptor-9 (TLR9; refs 1–5). It is also known that the formation of DNA–antimicrobial peptide complexes can lead to autoimmune diseases via amplification of pDC activation[1,2]. Here, by combining X-ray scattering, computer simulations, microscopy and measurements of pDC IFN production, we demonstrate that a broad range of antimicrobial peptides and other cationic molecules cause similar effects, and elucidate the criteria for amplification. TLR9 activation depends on both the inter-DNA spacing and the multiplicity of parallel DNA ligands in the self-assembled liquid-crystalline complex. Complexes with a grill-like arrangement of DNA at the optimum spacing can interlock with multiple TLR9 like a zipper, leading to multivalent electrostatic interactions that drastically amplify binding and thereby the immune response. Our results suggest that TLR9 activation and thus TLR9-mediated immune responses can be modulated deterministically.

TLR9 binding of DNA is complex and multifactorial[1–4]. Microbial DNA is typically transported into intracellular compartments during the process of infection and triggers IFN-α production in pDCs via the binding of unmethylated dinucleotide CG (CpG) motifs to endosomal TLR9. Host-derived (self)-DNA released in the context of cell death can also activate TLR9 in pDC via its sugar backbone[4], but this does not normally occur owing to the limited access of extracellular self-DNA to endosomal compartments[5]. However, in autoimmune diseases such as psoriasis[1] and lupus[2], self-DNA can form complexes with the antimicrobial peptide (AMP) LL37, and potently activate TLR9 in pDCs, leading to type I IFN production and disease exacerbation. Recent findings posed a significant challenge to understanding immune responses modulated by TLR9: other antimicrobial peptides, including human defensins HBD2 and HBD3 (ref. 6), as well as several chromatin-derived proteins, can form complexes with DNA and promote TLR9 binding[7] and activation[8,9]. One possibility is that complex formation can protect self-DNA from enzymatic degradation[10], and thereby enable endosomal access required for TLR9 receptor binding. However, this process is not sufficient for activation in pDCs, as other peptides complexed with DNA are unable to activate TLR9. At present, the selection criteria for TLR9 activation by complexed DNA are not understood.

Here, we show why a broad range of cationic molecules besides LL37 can complex with DNA and trigger interferon production in pDCs, whereas many other cationic molecules do not. We delineate the governing physical criterion for such high interferon secretion, by combining synchrotron small angle X-ray scattering (SAXS), fluorescence microscopy, computer simulations, and measurements of IFN-α production by pDCs. Both IFN-inducing and non-IFN-inducing cationic molecules form complexes with DNA and transport it into TLR9-containing endosomes of pDC. The key determinant for activation is the self-assembled structure of the liquid-crystalline peptide–DNA complex, especially the inter-DNA spacing between parallel DNA ligands. Using a coarse-grained computational model we show that electrostatic interactions between TLR9 and DNA are optimized when DNA columnar complexes have an inter-DNA spacing that is commensurate with the steric size of TLR9 receptors—allowing for 'interdigitation' of multiple receptors and ligands, like teeth in a zipper. The presentation of optimally spaced, parallel DNA ligands results in a new form of multivalent interaction[11] that drastically increases the number of active, ligand-bound receptors and thereby leads to potent IFN induction in pDCs.

We first assess the relationship between pDC activation and the structure of DNA complexes by using three prototypical examples of DNA–peptide complexes. Human immunodeficiency virus (HIV) transactivator of transcription (TAT) is a polycationic peptide that can penetrate cells[12] and gain endosomal access. We find that incubation of pDCs with TAT–DNA complexes does not produce significant levels of IFN-α in pDCs (Fig. 1). TAT–DNA complexes efficiently enter TLR9-containing endosomal compartments (Fig. 2b), however, suggesting that endosomal access is not sufficient for strong IFN induction in pDCs. SAXS measurements show that DNA is organized into a columnar arrangement within TAT–DNA complexes, similar to many phases of DNA (and other biological polyelectrolytes) condensed by multivalent cations[13]. Diffraction peaks from TAT–DNA complexes are observed at $q_{100} = 2.48\ \mathrm{nm}^{-1}$, $q_{101} = 3.08\ \mathrm{nm}^{-1}$ and $q_{110} = 4.41\ \mathrm{nm}^{-1}$ (Fig. 1a), characteristic of a columnar hexagonal lattice with parameters $a = 2.90$ nm, $c = 3.50$ nm (Fig. 3d)[14], which corresponds to a bundle-like complex with close-packed DNA. Like TAT peptide, human β-defensin-3 (HBD3) is polycationic, and is capable of condensing DNA and accessing TLR9 in endosomes. In contrast to

[1]Bioengineering Department, Chemistry & Biochemistry Department, California Nano Systems Institute, University of California, Los Angeles, California 90095, USA. [2]Hefei National Laboratory for Physical Sciences at Microscale, Department of Polymer Science and Engineering, CAS Key Laboratory of Soft Matter Chemistry, University of Science and Technology of China, Hefei 230026, China. [3]Department of Dermatology, Lausanne University Hospital CHUV, 1009 Lausanne, Switzerland. [4]Department of Infectious, Parasitic and Immunomediated Diseases, Istituto Superiore di Sanità, Rome 00161, Italy. [5]Department of Chemistry, University of Cambridge, Lensfield Road, CB2 1EW Cambridge, UK. [6]Department for Theoretical Physics, Jožef Stefan Institute, Jamova 39, 1000 Ljubljana, Slovenia. [7]International Center for Soft Matter Research, Beijing University of Chemical Technology, Beijing 100029, China. [†]These authors contributed equally to this work. *e-mail: jd489@cam.ac.uk; Michel.Gilliet@chuv.ch; gclwong.ucla@gmail.com

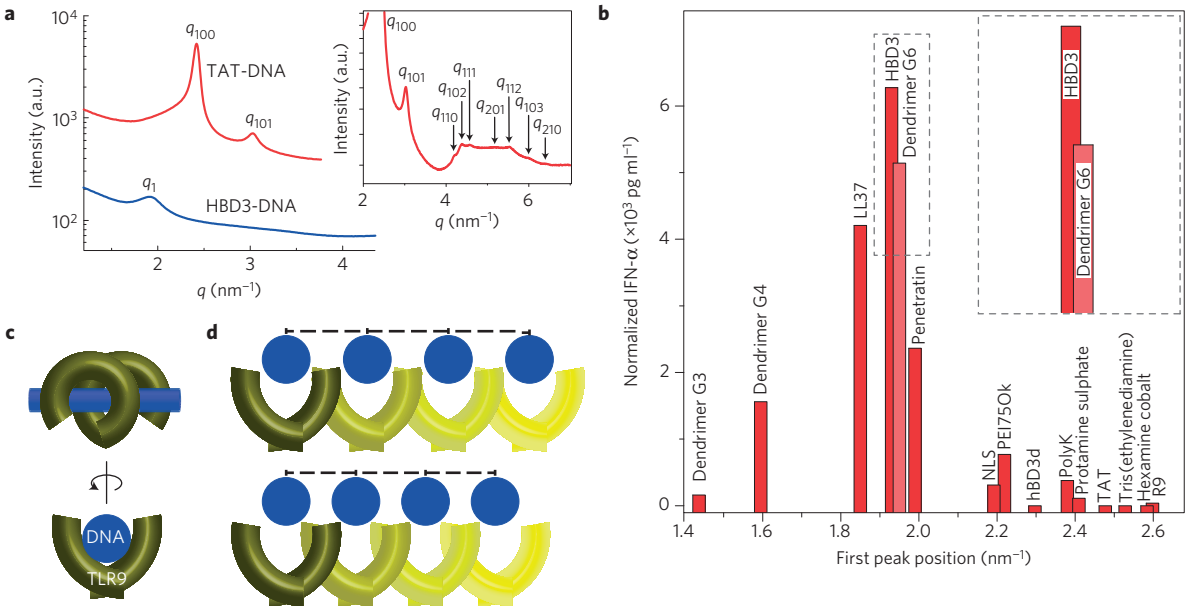

Figure 1 | Interferon IFN-α production in dendritic cells through TLR9 activation depends on DNA spacing in electrostatic DNA complexes formed with polycations. a, Representative SAXS data from peptide–DNA complexes that induce strong IFN-α production in dendritic cells (DNA with the antimicrobial peptide HBD3) and those that do not (DNA with TAT cell-penetrating peptide). Higher-order reflections for the TAT–DNA hexagonal lattice are shown in the upper right corner. **b**, IFN-α production by pDCs stimulated with polycation–DNA complexes, normalized for the amount of complex internalization, shows a strong correspondence with SAXS measurements of their first diffraction peak *q*-positions. As the first peak position is inversely proportional to the inter-DNA spacing, a narrow range of inter-DNA spacings result in high IFN-α production levels. Inset and shading are included to distinguish HBD3 and G6 bars. **c**, Illustration of the TLR9–dsDNA complex whose structure is unknown, based on the solved structure of (homologous) TLR3 complexed with dsRNA (refs 15,16). **d**, Different DNA spacings can impact TLR9 activation. Larger geometric spacings (top) between orientationally ordered DNA in the bundle can accommodate binding of multiple TLR9s and amplify activation, whereas smaller spacings (bottom) subdue activation because they sterically reduce accessibility of bundled DNA to receptors. Shading differences of adjacent TLR9 molecules indicate that they are offset along the columnar DNA lattice.

TAT peptide, HBD3–DNA complexes induce strong ~2,200 pg ml^{-1} IFN-α production in pDCs, which is roughly 100 times higher than IFN-α production from TAT–DNA complexes, consistent with extant results[6]. SAXS measurements (Fig. 1a) show that DNA within HBD3–DNA complexes also forms a columnar phase. A DNA correlation peak is observed at $q_{DNA} = 1.92\,nm^{-1}$, indicating that the inter-DNA spacing in HBD3–DNA complexes is 3.25 nm, which is considerably larger than the spacing in TAT–DNA complexes. Likewise, we find that LL37, which accesses TLR-containing endosomes (Fig. 2b) and induces high levels of IFN-α production in pDCs (Fig. 1b), also self-assembles with DNA into a columnar structure with an inter-DNA spacing $a_{DNA} = 3.40$ nm (Fig. 3a,b) significantly larger than the DNA diameter. These measurements suggest that the inter-DNA spacing in liquid-crystalline columnar DNA complexes correlates with induced IFN-α production by pDCs.

To test this hypothesis, we measured pDC activation for a broad range of self-assembled DNA complexes with different inter-DNA spacings by repeating the above analysis with a diverse set of natural and synthetic cationic agents, including peptides (R9, TAT, polylysine (MW ~ 70,000), human beta-defensin-3 derivative (hBD3d), nuclear localization sequence (NLS), penetratin, human beta-defensin-3 (HBD3), LL37) as well as non-peptide cationic molecules (hexamine cobalt, tris(ethylenediamine) cobalt, protamine sulphate, polyethylenimine polymer (average molecular weight 750 kDa; PEI750k), polyamidoamine (PAMAM) dendrimers (G3, G4, G6)) (Supplementary Table 1). SAXS measurements show these cationic agents condense DNA into ordered columnar complexes with a range of inter-DNA spacings from $a_{HexamineCo} = 2\pi/q_{HexamineCo} = 2.43$ nm for hexamine cobalt(III) to $a_{G3} = 2\pi/q_{G3} = 4.37$ nm for PAMAM dendrimer G3 (Fig. 1b). A crucial criterion for pDC activation in these DNA complexes is the inter-DNA spacing: strong IFN-α responses are induced by complexes with first peak positions between 1.8–2.0 nm^{-1} corresponding to inter-DNA spacings near $a \sim 3.5$ nm (Fig. 1b), whereas complexes with *a* spacings that deviate from this value induce weaker responses. Changes in salt levels over the range of physiological concentrations present in endosomes did not alter the structures of representative polycation–DNA complexes or their inter-DNA spacings to a degree sufficient to change activation profiles (Supplementary Fig. 2). Importantly, DNA complexed with polycations that induce strong and those that induce weak IFN-α responses both can access endosomes and co-localize with TLR9 (Fig. 2). The co-localization of non-inducing complexes with TLR9 demonstrates that cellular entry and trafficking cannot be solely responsible for their lack of activity. The efficiency of endosomal access may, in principle, modulate the degree of IFN-α response of polycation–DNA complexes that induce IFN-α production. These results show that the presentation of spatially periodic DNA with spacings comparable to the TLR receptor size can drastically increase IFN-α production by pDCs. The 'sweet spot' of 3–4 nm spacing is suggestive. The low-distance cutoff is roughly the steric size of TLR receptors[15–17], which defines the distance of closest approach between receptors. The large-distance cutoff is consistent with strong electrostatic interactions expected in this system, which allows anionic DNA to interact with both the inside and outside surfaces of adjacent cationic TLR9 receptors, and thereby 'crosslink' such receptors into a zipper-like ligand–receptor array (Fig. 1c,d). To test the plausibility of these explanations for the striking observations in Fig. 1, we will need to construct a suitable quantitative model.

Because a single ordered columnar DNA complex ('DNA bundle') can bind transversely and effectively present a spatially periodic 'grill'-like array of parallel DNA chains to multiple TLR9 receptors, there is potential for multivalent binding effects (Fig. 1d). The degree of multivalency can be estimated via the measured

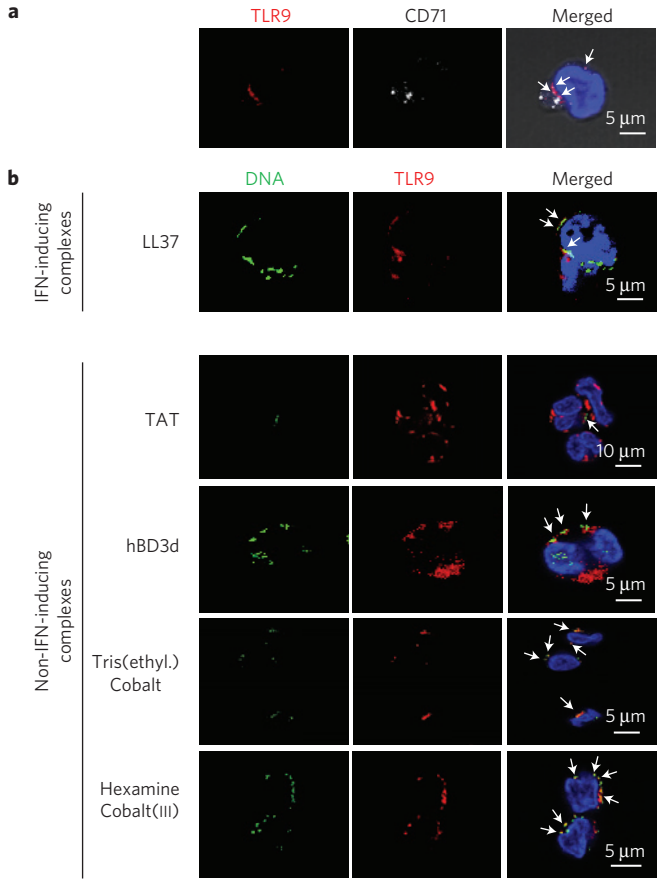

Figure 2 | Both IFN-inducing and non-IFN-inducing cationic molecules transport DNA to endosomal TLR9. PDCs were stimulated for 4 h with CpG-2006 (AlexaFluor^{488}) oligonucleotides complexed with either IFN-inducing (LL37) or non-IFN-inducing cationic molecules (hBD3d, TAT, tris(ethylenediamine) cobalt, hexamine cobalt(III)). Early endosomes were stained with AlexaFluor^{647}-labelled anti-transferrin receptor (CD71) along with an AlexaFluor^{546}-labelled anti-TLR9. Cell nuclei were stained with 4′,6-diamidino-2-phenylindole (DAPI) and the contour of the cells was visualized by transmitted light. **a**, Co-localization between TLR9 and endocytic compartments is shown by the arrows. **b**, DNA (AlexaFluor^{488}) complexed with IFN-inducing and non-IFN-inducing molecules co-localize with TLR9 (AlexaFluor^{546}), as highlighted by the arrows.

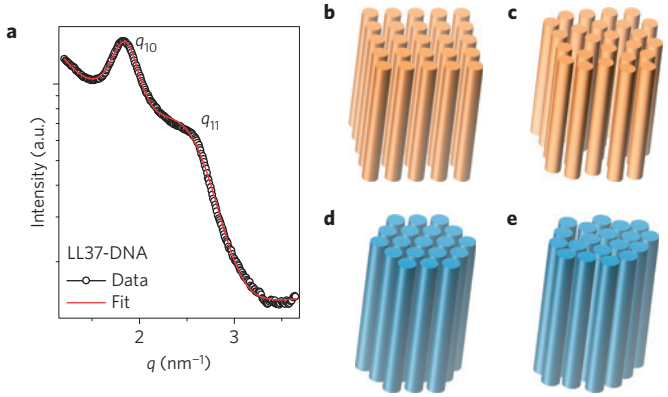

Figure 3 | The presentation of ordered columnar DNA complexes, with specific inter-DNA spacings. a, Representative SAXS spectra from LL37 complexed with DNA. Diffraction peaks are observed at $q_{10} = 1.85$ nm^{-1} and $q_{11} = 2.68$ nm^{-1}, which have the ratio 1: $\sqrt{2}$, characteristic of a square lattice with parameter $a = 3.40$ nm. The average linear domain size of LL37–DNA bundles is extracted from the fitted width, w, of the (10) peak (see SAXS data fits in Supplementary Information). **b**–**e**, Schematic representations of the four main structural types of DNA–polycation complexes observed in this study: the LL37–DNA columnar square lattice (**b**), the TAT–DNA columnar hexagonal lattice (**d**), and disordered columnar arrangements of DNA with larger inter-DNA spacing such as DNA complexed with HBD3 (**c**), or with smaller spacing that is consistent with DNA complexed with tris(ethylenediamine) cobalt (**e**). LL37–DNA complexes with inter-DNA spacings $a \sim 3.5$ nm induce much greater IFN-α production in pDCs compared with tightly packed TAT–DNA complexes with inter-DNA spacings of $a \sim 2.9$ nm.

domain size (Fig. 3a) of DNA ordering (Fig. 3b–e). Generally, in systems where ligands are able to form multiple weak bonds with target receptors, one can expect to observe 'super-selectivity'—that is, binding increasing sharply with receptor concentration[11]. Binding of immune complexes to TLR9 receptors is more complex, and depends sensitively on inter-DNA spacing in the bundle; we observe a drastic ~100-fold change in IFN-α production as the distance between DNA chains in a complex shifts ~0.5 nm. These systems are at present not accessible to all-atom simulations. Therefore, to investigate the origin of TLR9 amplification, we developed a coarse-grained computational model.

We first consider binding of TLR9 receptors to an isolated DNA chain. If there are κ available binding sites on DNA to which receptors can attach, the expected number of receptors, n_B, that are actually bound to the DNA is less than κ:

$$\frac{n_B}{\kappa} = \frac{e^{-\varepsilon/k_B T}}{1 + e^{-\varepsilon/k_B T}}$$

where ε is the binding free energy of receptors to DNA, which depends on DNA–TLR9 interactions and on the density of receptors on the membrane (see Model in Supplementary Information). In the case of weak binding, $e^{-\varepsilon/k_B T} \ll 1$, this simplifies to $n_B \approx \kappa e^{-\varepsilon/k_B T}$. For $\varepsilon \approx 4k_B T$, the TLR9 receptors will cover less than 2% of an isolated DNA chain. When DNA chains are arranged into a bundle, however, the electrostatic interactions between TLR9 molecules and DNA are different: each cationic TLR9 molecule can now interact with three anionic DNA chains (Fig. 4a), the one in the TLR9 binding groove, and the two immediately adjacent to it. The effective binding free energy is then

$$\varepsilon^* = \varepsilon + 2U(a)$$

where $U(a)$ is a sum of all additional interactions between a TLR9 molecule and an adjacent DNA chain (electrostatic interaction is represented by the screened Yukawa potential and steric repulsion between TLR9 and DNA by the repulsive term of the 12-6 Lennard-Jones interaction, see Model in Supplementary Information and Supplementary Fig. 4). The binding free energy ε^* to a bundle decreases (binding becomes stronger) when the spacing between DNA is reduced—until the spacing is so small that steric effects become important. The binding is strongest for commensurately spaced DNA chains that allow 'interdigitation' between TLR9 and the periodic DNA array, where multiple receptors and ligands interlock in an alternating manner. Such optimal ordered structures can recruit and bind many TLR9 molecules (Fig. 4b and Supplementary Fig. 4) and trigger an order of magnitude stronger pDC response than the mismatched structures.

To test this hypothesis, we performed Monte Carlo simulations to determine the equilibrium number of bonds, $n_B(a)$, formed between TLR9 receptors and a DNA array with set ligand number $\kappa = 6$ (extracted from the LL37–DNA domain size, Fig. 3a) and given spacing a. For strong binding ($\varepsilon < 2k_B T$), the number of formed bonds does not depend strongly on DNA spacing; n_B is appreciable for expanded bundles with large a. This regime is inconsistent with our observations (Fig. 1b) because bundles with large a

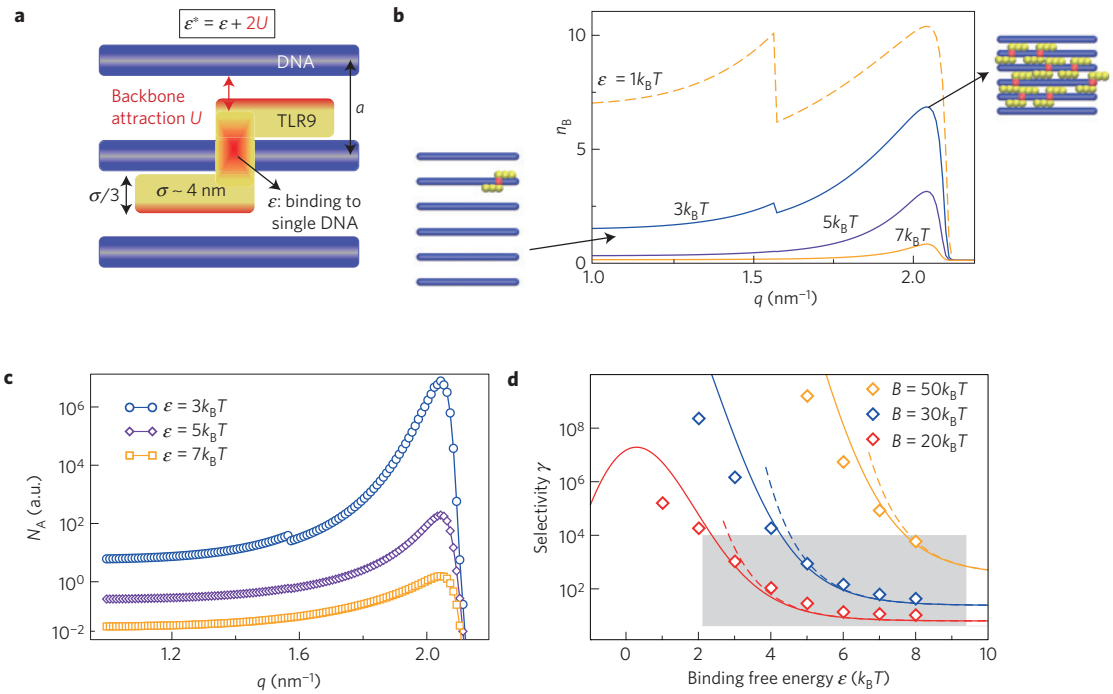

Figure 4 | Coarse-grained model of TLR9 binding to DNA bundles exhibits 'super-selective' behaviour in agreement with experimental observations. **a**, Schematic representation of the model: DNA are uniformly charged rods arranged in an ordered 'grill'-like array with lattice spacing a. This mimics a DNA bundle binding to receptors on a membrane sideways. TLR9 are represented in projection as S-shaped 'tetris blocks' with two arms of length σ, width $\sigma/3$, and uniform charge density opposite to that of DNA. **b**, Equilibrium number of bonds, n_B, as a function of inverse lattice spacing $q=2\pi/a$, for various binding free energies ε, at TLR9–DNA electrostatic interaction $B=AZ_1Z_2k_BT=30k_BT$, where $Z_{1,2}$ are effective charges and A is a constant. Two simulation snapshots from $\varepsilon=3k_BT$ further illustrate bond statistics. **c**, Total number of active receptors, N_A, as a function of q at $B=30k_BT$. Multivalency increases the lattice-spacing-selective response. **d**, The peak-to-plateau ratio, $\gamma=N_A(a^*)/N_A(\infty)$, characterizing the degree of selectivity (see Supplementary Note 8). Symbols are from numerical simulations; solid lines represent the Langmuir theory, and dashed lines are a double-exponential approximation to the full theoretical expression (see Analytical theory in Supplementary Information). Large γ are observed over a range of different B and ε. Grey shaded area marks the parameter values that correspond to experiments.

(small q) do not induce high amounts of IFN-α production (see Supplementary Note 7). In the weak binding scenarios, $\varepsilon=3k_BT$, $5k_BT$ and $7k_BT$, the curves follow the experimental trend and exhibit a pronounced maximum at $2\pi/a^*\approx2\,\mathrm{nm}^{-1}$ (Fig. 4b), corresponding to the optimal lattice spacing $a^*\approx3$ nm. These conditions approach the close-packing limit for DNA chains and TLR9. At smaller spacing, steric repulsion prevents binding and leads to the sharp decrease in n_B. Therefore, the self-organization of an interlocking receptor–ligand array strongly enhances binding of DNA bundles to TLR9 receptors.

The single TLR9–DNA bonds are relatively weak, but their number n_B increases significantly with the decreasing lattice spacing—up to a ratio $n_B(a^*)/n_B(\infty)$ of approximately 5 to 10. The possibility to form many weak bonds greatly increases the combinatorial entropy and thus decreases the free energy $F(a)$ for DNA bundles binding to the receptor-decorated membrane. The number of all active (that is, bound to DNA) receptors is determined by the product of the number of bound DNA bundles and the average number of bonds each bound bundle makes with receptors:

$$N_A(a)\propto n_B e^{-F(a)/k_BT}$$

Accounting for these different layers of statistical mechanical effects from multivalent binding, one can clearly see (Fig. 4c) that the response of the cell from receptor activation, $N_A(a)$, becomes strongly amplified. This can be seen in a Langmuir-like analytical model (see Analytical theory in Supplementary Information) that predicts exponential scaling of $n_B(a)$ with the binding strength, whereas the total activation $N_A(a)$ shows a much stronger double-exponential dependence[18]. The degree of selectivity can be defined as a ratio of cell activation in optimally condensed ($a=a^*$) and expanded ($a\to\infty$) bundles:

$$\gamma^A\equiv\frac{N_A(a^*)}{N_A(\infty)}$$

Experimental observations predict $\gamma\approx100$ (Fig. 1b), which agrees with numerical simulations and theory based on this plausibility model with a reasonable choice of parameters (Fig. 4d). Moreover, these results are robust: the same trends are observed qualitatively when effects from monovalent salt (Supplementary Fig. 5) and noise (allowing the DNA to diffuse about their average position in the two-dimensional (2D) lattice) (Supplementary Fig. 6) are incorporated into the simulations.

The simplified quantitative model above strongly suggests that electrostatic self-assembly between DNA, cationic ligands, and TLR9 can drive a drastic amplification of the number of active receptors. Importantly, TLR9 activation depends on both the inter-DNA spacing and the number of DNA ligands in the complex, as both factors contribute strongly to multivalency and binding amplification. The above effects can operate in concert with other processes, such as protection from enzymatic degradation[10], receptor cooperativity[19], and downstream consequences of active TLR9 receptors.

In vitro experiments have used cationic liposomes to form DNA complexes that are internalized in dendritic cells and transfected cell lines to modulate TLR9 activation[1,6,20], but the microscopic mechanism is not understood. Consistent with our model, cationic lipids can also organize DNA into a rich polymorphism of spatially periodic structures, including 2D lamellar structures with

tunable inter-DNA spacings[21,22]. The emerging picture implies that pDC activation is not deterministically controlled by uncorrelated binding between individual ligands and receptors; rather, the induced organization of immune ligands into optimal periodic structures can result in massive binding enhancement, and thereby strongly amplify immune response.

Although our explanatory model is relatively simple, the empirical results described here have broad implications for controlling the immune response. It will be interesting to determine whether natural AMPs can bind to and organize DNA fragments from permeated pathogens, and thereby enable multivalent presentation to TLR9 and promote adaptive immune responses. As TLR9 activation is highly sensitive to inter-DNA spacing in ordered electrostatic complexes, knowledge of their structures can inform immunotherapies. The data here suggest that cationic proteins, peptides, or other cationic agents less than 0.5 nm in size or greater than 2.0 nm in size do not activate TLR9, as steric constraints will prevent them from forming a TLR9–DNA zipper. The behaviour of cationic proteins or peptides in the intermediate size regime between 0.5 nm and 2.0 nm can be engaged via straightforward computer simulations[23] if the structures are known, as electrostatic binding in aqueous environments depends on charge distribution, shape, and binding orientation of the protein. Importantly, these results suggest that TLR9 activation can be attenuated by engineering the inter-DNA spacing to suppress the receptor–ligand zipper arrays via competitive binding, and potentially suppress inflammation in autoimmune diseases such as psoriasis. Likewise, by leveraging the fundamental understanding of electrostatic self-assembly[23,24], we can deterministically trigger immune responses in the context of vaccines, and predict which synthetic nano-sized objects are likely to induce adventitious inflammatory response, with strong implications for nanotoxicology.

Methods

Methods and any associated references are available in the online version of the paper.

Received 20 May 2014; accepted 20 April 2015; published online 8 June 2015

References

1. Lande, R. *et al.* Plasmacytoid dendritic cells sense self-DNA coupled with antimicrobial peptide. *Nature* **449,** 564–569 (2007).
2. Lande, R. *et al.* Neutrophils activate plasmacytoid dendritic cells by releasing self-DNA–peptide complexes in systemic lupus erythematosus. *Sci. Transl. Med.* **3,** 73ra19 (2011).
3. Hemmi, H. *et al.* A Toll-like receptor recognizes bacterial DNA. *Nature* **408,** 740–745 (2000).
4. Haas, T. *et al.* The DNA sugar backbone 2′ deoxyribose determines Toll-like receptor 9 activation. *Immunity* **28,** 315–323 (2008).
5. Barbalat, R., Ewald, S. E., Mouchess, M. L. & Barton, G. M. Nucleic acid recognition by the innate immune system. *Annu. Rev. Immunol.* **29,** 185–214 (2011).
6. Tewary, P. *et al.* β-Defensin 2 and 3 promote the uptake of self or CpG DNA, enhance IFN-α production by human plasmacytoid dendritic cells, and promote inflammation. *J. Immunol.* **191,** 865–874 (2013).
7. Li, Y., Berke, I. C. & Modis, Y. DNA binding to proteolytically activated TLR9 is sequence-independent and enhanced by DNA curvature. *EMBO J.* **31,** 919–931 (2012).
8. Tian, J. *et al.* Toll-like receptor 9-dependent activation by DNA-containing immune complexes is mediated by HMGB1 and RAGE. *Nature Immunol.* **8,** 487–496 (2007).
9. Yanai, H. *et al.* HMGB proteins function as universal sentinels for nucleic-acid-mediated innate immune responses. *Nature* **462,** 99–103 (2009).
10. Gilliet, M. & Lande, R. Antimicrobial peptides and self-DNA in autoimmune skin inflammation. *Curr. Opin. Immunol.* **20,** 401–407 (2008).
11. Martinez-Veracoechea, F. J. & Frenkel, D. Designing super selectivity in multivalent nano-particle binding. *Proc. Natl Acad. Sci. USA* **108,** 10963–10968 (2011).
12. Brooks, H., Lebleu, B. & Vivès, E. Tat peptide-mediated cellular delivery: Back to basics. *Adv. Drug Deliv. Rev.* **57,** 559–577 (2005).
13. Evans, H. M. *et al.* Structural polymorphism of DNA-dendrimer complexes. *Phys. Rev. Lett.* **91,** 075501 (2003).
14. DeRouchey, J., Netz, R. & Rädler, J. Structural investigations of DNA-polycation complexes. *Eur. Phys. J. E* **16,** 17–28 (2005).
15. Choe, J., Kelker, M. S. & Wilson, I. A. Crystal structure of human Toll-like receptor 3 (TLR3) ectodomain. *Science* **309,** 581–585 (2005).
16. Liu, L. *et al.* Structural basis of Toll-like receptor 3 signaling with double-stranded RNA. *Science* **320,** 379–381 (2008).
17. Kang, J. Y. & Lee, J-O. Structural biology of the Toll-like receptor family. *Annu. Rev. Biochem.* **80,** 917–941 (2011).
18. Geerts, N. & Eiser, E. DNA-functionalized colloids: Physical properties and applications. *Soft Matter* **6,** 4647–4660 (2010).
19. Luo, J. *et al.* Lateral clustering of TLR3: dsRNA signaling units revealed by TLR3ecd: 3Fabs quaternary structure. *J. Mol. Biol.* **421,** 112–124 (2012).
20. Honda, K. *et al.* Spatiotemporal regulation of MyD88–IRF-7 signalling for robust type-I interferon induction. *Nature* **434,** 1035–1040 (2005).
21. Koltover, I., Salditt, T., Rädler, J. O. & Safinya, C. R. An inverted hexagonal phase of cationic liposome-DNA complexes related to DNA release and delivery. *Science* **281,** 78–81 (1998).
22. Rädler, J. O., Koltover, I., Salditt, T. & Safinya, C. R. Structure of DNA-cationic liposome complexes: DNA intercalation in multilamellar membranes in distinct interhelical packing regimes. *Science* **275,** 810–814 (1997).
23. Sanders, L. K. *et al.* Control of electrostatic interactions between F-actin and genetically modified lysozyme in aqueous media. *Proc. Natl Acad. Sci. USA* **104,** 15994–15999 (2007).
24. Wong, G. C. & Pollack, L. Electrostatics of strongly charged biological polymers: Ion-mediated interactions and self-organization in nucleic acids and proteins. *Annu. Rev. Phys. Chem.* **61,** 171–189 (2010).

Acknowledgements

This work is supported by NSF grants DMR1411329 and DMR1106106, EU grants ARG-ERC-COLSTRUCTION 227758 and ITN-COMPLOIDS 234810, by the Herchel Smith Fund, and by the Slovenian Research Agency through Grant P1-0055, and the Swiss National Science Foundation (FN 310030-144072). X-ray research was conducted at Stanford Synchrotron Radiation Lightsource, SLAC National Laboratory, supported by the US DOE Office of Basic Energy Sciences under Contract No. DE-AC02-76SF00515, the Advanced Light Source, supported by the US DOE Office of Basic Energy Sciences under Contract No. DE-AC02-05CH11231, and at the UCLA CNSI.

Author contributions

G.C.L.W., M.G., F.J. and N.W.S. conceived the project. R.L. and L.F. performed the cell experiments. F.J., N.W.S., W.X. and C.L. performed SAXS experiments. N.W.S., F.J. and C.L. analysed SAXS data. T.C., J.D. and D.F. conceived the computational model. T.C. performed simulations. G.C.L.W., N.W.S., M.G., D.F., J.D. and T.C. wrote the manuscript. F.J. and R.L. assisted with the methods section.

Additional information

Supplementary information is available in the online version of the paper. Reprints and permissions information is available online at www.nature.com/reprints. Correspondence and requests for materials should be addressed to J.D., M.G. or G.C.L.W.

Competing financial interests

The authors declare no competing financial interests.

Methods

Self-assembled DNA complexes preparation. For SAXS, monodispersed Lambda DNA (BioLabs) is precipitated and resuspended in aqueous solution, at 100 mM NaCl or a buffer composed of 10 mM HEPES and 100 mM NaCl adjusted to pH = 7.4, 5.4 or 5.0, depending on the condensing agent. Self-DNA was used in the cell experiments. Peptide-based cationic agents (≥95% purity, Anaspec) include: R9 (RRRRRRRRR), poly K (MW ~ 70,000), TAT (YGRKKRRQRRR), hBD3d derivative (KSSTRGRKSSRRKK), NLS (PKKKRKV), ANTP Penetratin (RQIKIWFQNRRMKWKKGG), HBD3 (GIINTLQKYYCRVRGGRCAVLSCLPK EEQIGKCSTRGRKCCRRKK), and human LL37 (LLGDFFRKSKEKIGKE FKRIVQRIKDFLRNLVPRTES). Non-peptide-based cationic agents include cobalt hexamine, cobalt tris(ethylenediamine), protamine sulphate, Polyethyleneimine (M_W ~750,000), PAMAM dendrimer (G3, G4, G6), which are all used without further purification. Complexes were formed between each cationic agent and DNA by incubating the agent with DNA (10 mg ml^{-1} for SAXS, 10 μg ml^{-1} for cells) at specific charge ratios. For a given cationic agent the same charge ratios were used in both SAXS and cell experiments.

Cell experiments. pDC isolation and stimulation. Human blood pDCs were isolated from buffy coats obtained from the blood of healthy donors at the Service Regional Blood Bank. After separation of mononuclear cells by Ficoll centrifugation, pDCs were purified by using a PDC negative selection cocktail (Plasmacytoid Dendritic Cell Isolation Kit II) to reach 99% purity. Purified pDCs were seeded into 96-well round-bottom plates at 5×10^4 per well in 200 μl RPMI 1640 (GIBCO) supplemented with 10% fetal calf serum (FCS) (Atlanta Biologicals). Supernatants of stimulated pDCs were collected after overnight culture. Cytokine levels in the supernatants were determined by using ELISA kits for human IFN-α (PBL Biomedical Laboratories).

Uptake of complexes. Uptake of DNA complexes by pDCs was visualized by using human DNA (BioChain) labelled with AlexaFluor^{488} by using the Ulysis Nucleic Acid Labelling Kit (Molecular Probes), according to the standard protocol provided by the manufacturer, as previously described. After 4 h of pDC stimulation with DNA–Alexa^{488}-containing complexes, stimulated pDC were washed and the percentage of Alexa^{488}-positive cells was determined by flow cytometry. Self-DNA was used at 10 μg ml^{-1}.

Normalized IFN-α production. To provide a more accurate view of the ability of DNA complexes to trigger endosomal TLR9 activation, IFN-α levels were normalized by the percentages of pDC that have actually internalized the complexes. The normalization controls for variations in IFN-α production due to variations in the uptake of these complexes by pDCs. Uptake of DNA complexes was conducted as described in 'Uptake of complexes'.

Cell staining and imaging of endosomal trafficking. pDCs were stimulated with AlexaFluor^{488}-labelled CpG 2006 (Trilink) in complex with the following cationic peptides: LL37, hBD3d, TAT_{46-60}, and non-peptide cationic molecules: tris(ethylenediamine) cobalt, hexamine cobalt. Cells were washed after 1 h of stimulation and further incubated for a total of 4 h, transferred onto coverslips pretreated with polylysine, fixed for 15 min in 4% para-formaldehyde, and permeabilized in PBS supplemented with 0.5% Triton X 100 (Sigma-Aldrich) and 1% normal goat serum (Jackson ImmunoResearch Laboratories). Samples were then stained with a rat anti-human TLR9 (CD289) (eBiosciences) antibody together with a mouse anti-human transferrin-receptor (CD71) (eBiosciences) monoclonal antibody followed by AlexaFluor^{546}-labelled anti rat (Invitrogen) and AlexaFluor^{647}-labelled anti-mouse (Life Technologies) in permeabilization buffer. Slides were washed and mounted in Prolong Gold antifade mounting media (Molecular Probes) before imaging.

Imaging was performed using a Zeiss LSM 710 laser scanning confocal microscope with an oil immersion objective (×63/1.4 numerical aperture).

SAXS experiments. SAXS measurements. We measure a phase diagram for complexes formed between each cationic agent and DNA, by incubating them with DNA (10 mg ml^{-1}) at specific charge ratios. After thorough mixing and centrifugation, the complexes are hermetically sealed in 1.5 mm quartz capillaries (Hilgenberg GmbH, Mark-tubes, Code No: 4017515, and Charles Supper). SAXS measurements were performed at beamline 4–2 of the Stanford Synchrotron Radiation Laboratory (SSRL). Monochromatic X-rays with energies 9–12 keV were used. A Rayonix MX225-HE detector (pixel size 73.2 × 73.2 μm) was used to collect the scattered radiation. Samples were also measured using the California NanoSystems Institute (CNSI) SAXS spectrometer at UCLA (incident wavelength, $\lambda = 1.54$ Å) and a MAR345 image plate detector (pixel size 150 × 150 μm). Identical samples were prepared and measured at different times after preparation using multiple light sources to ensure consistency in data. The 2D SAXS powder patterns were azimuthally integrated using the Nika 1.48 package (http://usaxs.xor.aps.anl.gov/staff/ilavsky/nika.html) for Igor Pro 6.22 and Fit2D (http://www.esrf.eu/computing/scientific/FIT2D).